Stress Distribution of Metatarsals during Forefoot Strike versus Rearfoot Strike: a Finite Element Study

Shudong Li[1,2,3], Yan Zhang[1,2,4], Yaodong Gu[1,2*], James Ren[3]

[1]Faculty of Sports Science, Ningbo University, China

[2] Research Academy of Grand Health Interdisciplinary, Ningbo University, China

[3] Faculty of Engineering and Technology, Liverpool John Moores University, UK

[4] Department of Automation, Biomechanics and Mechatronics, The Lodz University of Technology, Poland

*Corresponding Author: Yaodong Gu

E-mail Address: guyaodong@nbu.edu.cn

Address: Faculty of Sports Science, Ningbo University, No. 818, Fenghua Road, Jiangbei District, Ningbo, Zhejiang Province, China.

Abstract:
Due to the limitations of experimental approaches, comparison of the internal deformation and stresses of the human man foot between forefoot and rearfoot landing is not fully established. The objective of this work is to develop an effective FE modelling approach to comparatively study the stresses and energy in the foot during forefoot strike (FS) and rearfoot strike(RS). The stress level and rate of stress increase in the Metatarsals are established and the injury risk between these two landing styles is evaluated and discussed. A detailed subject specific FE foot model is developed and validated. A hexahedral dominated meshing scheme was applied on the surface of the foot bones and skin. An explicit solver (Abaqus/Explicit) was used to stimulate the transient landing process. The deformation and internal energy of the foot and stresses in the metatarsals are comparatively investigated. The results for forefoot strike tests showed an overall higher average stress level in the metatarsals during the entire landing cycle than that for rearfoot strike. The increase rate of the metatarsal stress from the 0.5 body weight (BW) to 2 BW load point is 30.76% for forefoot strike and 21.39% for rearfoot strike. The maximum rate of stress increase among the five metatarsals is observed on the 1st metatarsal in both landing modes. The results indicate that high stress level during forefoot landing phase may increase potential of metatarsal injuries.

Keywords: Finite element analysis, metatarsal stress, forefoot strike, rearfoot strike

INTRODUCTION

Foot strike pattern is a major issue influencing the lower extremity biomechanics during running. Forefoot strike and rearfoot strike are two common landing styles of running [1, 2]. In a forefoot strike, the ball of foot impacts with the ground first, during which, the foot was initially landed with a plantarflexion posture, followed by a dorsiflexion movement. Compared to rearfoot strike, forefoot strike cuts down the impact and reduces the shock passing to the brain as the impact is absorbed by the compression of the foot arch, eccentric contraction of the triceps surae, calf muscles and Achilles tendon stretch [3]. The pressure excursion during forefoot strike that moves backward was once considered to be an energy waste but was later proven to provide cushioning for runners [4]. Recent researches showed that the vertical loading rate of a habitual barefoot runner can be significantly reduced by changing the landing pattern from rearfoot strike to non-rearfoot strike [5, 6].

In the work by Lieberman [3], no obvious impact transient was found in the typical force-time data of forefoot strike. Conversely, the force-time curve of classic rearfoot strike always shows an impact transient before the vertical ground reaction approaches its peak. During the impact period of a rearfoot landing, the vertical Ground Reaction Force (GRF) can be 3 times higher than that for forefoot landing of habitual barefoot runners [3]. In rearfoot strike running, impact absorption is limited to the rearfoot pad and the shoe, leading to a higher peak impact, generating a shock wave, This could lead to high stress and strain directly contributing to injuries [7]. This is one of the reasons that running in minimalist footwear has been considered as a mean to reduce or eliminate running injuries by returning to a more natural gait.

A forefoot landing style put metatarsals at the first place of impact, in which the metatarsal bones would bear more load compared to the load level in a rearfoot strike or midfoot landing styles. This has been proved to be the case by insole pressure loading measurement [8]. In addition, it was also reported that the GRF and plantar pressure under the metatarsals were greater in the forefoot and phalanges during non-rear foot strike [8]. Running in a forefoot landing pattern may also increase the potential of metatarsal injuries such as fracture. Recent case studies revealed that the use of minimalist footwear by novices with a habit of rearfoot strike, could cause higher occurrence of metatarsal stress fractures [9, 10].

In order to understand the biomechanical mechanism of metatarsal injuries, it is important to quantify the internal stresses. Numerical modelling provides the prediction

of internal stress distribution of the foot under different loading conditions. FEM is commonly used in many biomechanical investigations with great success due to its ability to model complex material properties and irregular geometry as well as the capacity of simulating the internal stress in bones and tissue. Many published studies have focused on the foot stress under static standing load [11-13]. Stress in the bony foot structure was simulated during balance standing by Cheung noting a clear effect of the soft tissue stiffening and of the use of different types of foot support design [12, 13], including the modelling of foot with medical conditions such as diabetic foot [14]. Edwards et al. successfully used a probabilistic model coupled with the FE method to estimate the probability of stress fracture under a training scheme in which subjects ran at 3.5 and 4.5m/s over a period of 100 days [15].

In both cases, forefoot or rearfoot strikes, the high intensity impact induced when landing is a major factor for potential injury of foot bones or soft tissues. A comparative study of the foot deformations in these two landing phases will provide important data and impact characteristics within the relatively short time between foot-ground interaction. The improved understanding of the impact process simulated by FEM can also provide the information for enhancing the protection of the foot, designing devices embedded in shoe sole for smart shoes or implanted sensors. Wearable technology has been a popular topic in the field of public health science, with more and more footwear set a space aside for embedding a sensor to record plantar pressure and even foot movement in gait. The impact during landing is the most vulnerable phase for the sensors among the whole gait cycle. Consideration of different landing styles (i.e. forefoot and rearfoot strike) in the design of embedded or implanted sensors is necessary to balance the function of the sensors such as shoe sole stiffness, sensor reliability and wearing experience for the users with different strike patterns.

The purpose of this study is to investigate the internal stresses in metatarsals during forefoot and rearfoot strike. The stress level and stress increase rate in the metatarsals during a forefoot strike would be higher in forefoot strike than that for rearfoot strike and FEA will help to quantify these differences.

FE MODEL AND METHODS

Morphometrical analysis: virtual solid and finite element models

The subject-specific FE foot model was acquired by the reconstruction of 3D Computer Tomography (CT) and Magnetic resonance imaging (MRI) images of a male subject (age: 26, height: 180 cm, weight: 70 kg and foot length: 265 mm foot length). The subject is healthy without any known injury or foot problem in the past 3 years. Coronal CT images were taken with a space interval of 2 mm in the neutral unloaded position. The images of 28 bones (i.e. talus, calcaneus, cuboid, navicular, 3 cuneiforms, 5 metatarsals, and 14 components of the phalanges) and an encapsulated volume were segmented using MIMICS 16.0 (Materialise, Leuven, Belgium) together with the cartilages between bones to obtain the boundaries of the skeleton and exterior surfaces for assembling the model in .STL format. Coronal MR (magnetic resonance) imaging (Philips Achieva) of the same supine volunteer was used to segment the detail dataset with a lower density than the bones (soft tissue, cartilage, skin, and ligament) acquired at a slice thickness of 1.5mm (200 slices) and pixel spacing of 0.8594 mm from 256 × 256 captured pixels while the foot is at a natural unload state (ankle angle90°).

Solidworks (SolidWorks Corporation, Massachusetts) was used to convert all volume into solid parts in the format of .STEP files. Each part of bone was partitioned (see the flow chart in Fig. 1) in order to assign brick elements with gradual changes in the cross section between each partitioned cell based on its anatomy structure. Most of the published FE foot models were meshed by tetrahedral element due to the limitation of common FE packages such as Abaqus and Ansys in order to cope with the highly irregular shapes of the parts. In this work, the foot model was properly partitioned based on the anatomical features and meshed in Hypermesh (13.0), in which hexahedral elements can be applied on the irregular geometries such as bones and other organs. The number of hexahedral elements applied to solid bones and foot is highly dependent on the quality of the partitions. In this model, 90% of the surface layers of the foot and bones was successfully meshed by hexahedral elements which provide a smooth foot-floor interaction during striking with much high local accuracy and use less elements compared to that of a model solely with tetrahedral elements. In all other parts, hexahedral and tetrahedral elements were jointly employed, in which the aspect ratio of the brick elements was close to 1, this approach could improve the local accuracy of the FE model. All elements were imported into the commercial FE package Abaqus (6.14) as an .INP file to apply the loading and boundary conditions before simulation

and analysis mimicking forefoot landing and rearfoot strike. Two types of elements have been used in the main structure of the final foot model: four-node tetrahedral element (C3D4) elements and general purpose linear brick elements (C3D8R) with reduced integration. Use of reduced integration in Abaqus explicit could help dealing with incompressible behaviours. Detailed meshes sensitivity tests have been conducted in the preliminary work by gradually reducing the element sizes until the difference of resulted force-displacement data between two meshes is within 3%. The final model consists of 273123 elements. Due to the impact character of the foot landing and small time step required, Abaqus explicit solver is used [16-19]. A recent published work [16] used explicit solver for a 2D foot model. In previous works, Abaqus explicit solver has been used for modelling indentation of soft materials and deformation of structures embedded in a soft matrix and many other soft material systems [17, 18, 19, 20, 21]. For a 3D foot model with complex bony structures and different components of soft tissues, an explicit solver offers a more efficient choice for dealing with contact and impact [22]. One key issue is the achievement of stability/convergences of the model, which is controlled by the damping factor and/or mass scaling. Many key factors have been properly developed including mesh, mass, damping, contact as well calculation step. Further details will be presented in the boundary and loading conditions and convergence studies.

Materials Properties

A range of material properties and models are used for different foot structures and parts. An analytical rigid plate was used to represent the ground to simulate the foot–ground interaction during landing. This is close to the biomechanical testing condition, it is also representative of a more damaging situation to the metatarsals. The bones are defined as a linear elastic isotropic material (Young's Modulus=7300 MPa, Poisson's ratio=0.3) [23]. As in previous works [11] and other literatures [24], the stiffness of the Cartilage, Plantar Fascia and Ligament is set at 1, 350 and 250 MPa, respectively; the Poisson's ratio is set as 0.4. The phalanges are assumed to have the same material properties as the bones [16]. The density for the bone is 1500kg/m^3, the density of the tissue is 940 kg/m^3. A Rayleigh material damping coefficient (alpha) 6.7 was defined to represent the viscous behaviour of the soft tissue in ABAQUS [16]. The remaining soft tissues which encapsulated the bony structures was described by a hyperelastic model with a second-order polynomial strain energy potential obtained from *in vivo* ultrasonic measurements [25].

$$U = \sum_{i+j=1}^{2} C_{ij}(\overline{I_1} - 3)^i(\overline{I_2} - 3)^i + \sum_{i=1}^{2} \frac{1}{D_i}(J_{el} - 1)^{2i}$$

Where U is the strain energy per unit reference volume; C_{ij} and D_i are material parameters. J is the volume ratio; I_1 and I_2 are the first and second deviatoric strain invariants. The coefficients of the hyperelastic material used for the encapsulated soft tissue is C_{10}=0.08556, C_{01}=-0.0841, C_{11}=-0.02319, C_{02}=0.00851, D_1 = 3.65273, D_2=0. [11, 25]. The data was obtained through an *in vivo* compression measurement with several cohorts and inverse parameter fitting, the model had been used in serval published biomechanical works [11, 12, 13]. When D_2=0, it represents full incompressibility. Theoretically incompressibility can cause volume locking. For linear elastic models, this can be practically dealt with by using a Poisson's ratio close to 0.5. For hyperelastic model, full volume locking with an incompressible material can be avoided by using elements with reduced integrations. High quality meshes are also important for dealing with modelling problem due to incompressible behaviours [26].

Boundary, loading conditions and convergence studies

The main bony foot components were embedded in the encapsulated soft tissue volume using "Constraint of Embedded Region" [26] The procedure used constraint type of "Embedded Region" to model the interaction between the thin layer within the "whole model". This approach allows the user to insert a structure within a "host" region of the model or within the whole model [26]. The overall bony foot structure was treated as the embedded elements. This is an effective approach in dealing with multiple components system such as embedded systems structures in soft matrix [18]. In the model, the displacement-history data from kinematical experiments was applied on the cross section of tibia and fibula, following the displacement-history obtained from biomechanical tests using high speed camera and reflective markers. This is more realistic loading with an explicit solver to compare forefoot and rearfoot strike, rather than moving the plate upwards as used in other publications [27, 28]. The collision force of touching down is 1.5-3 times of the body weight [3]. Full contact was defined between the foot surface and the ground, with a surface to surface contact condition and the friction coefficient between foot plantar and the rigid plate was 0.6 [11, 16, 29]. Foot deformation under static standing load is usually simulated by standard implicit solver. For example, Gu [11] built a full foot model to compare the effect of different mat thicknesses on the metatarsal stress by using the standard solver. However, during running gait, the time period of landing will dramatically affect the result of GRF, plantar pressure, and stresses, etc., therefore, explicit Solver (Abaqus/Explicit) was

used to avoid convergence problem. The time period of landing phase was also considered, it took 0.1s from half body weight to reach twice body weight. The displacement history on the foot is applied as kinematical data of ankle (including tibia and fibula) following the displacement-time captured by a high-speed camera system. In the experimental work, we used reflective markers to record the displacement of the ankle and deformation of the foot. The averaged displacement history at top surface of the model (including tibia, fibula and soft tissue) was used to control the foot landing in the model, this is more realistic than moving the plate [27, 28, 30]. The initial touchdown angle in forefoot and rearfoot strike between the foot plantar and the ground was defined as 5° by gait measurement with reflective markers. Convergence studies are influenced by the mesh quality, linear damping parameters and time steps used, etc. We have evaluated the effect of the damping parameters using a trial and error process to minimise the ground reaction force oscillations. In the meantime, as a unique problem of the foot structure, the continuity (localized instability) of the foot deformation is also analysed as the system consists of regions with significantly different material properties. The final value consists of a linear bulk viscosity parameter of 0.035 and a quadratic bulk viscosity parameter of 0.6. The minimum target time increment is set at 1E-7, which is found to be applicable to all the three loading conditions (i.e. standing, forefoot landing and rear foot landing). These parameters combined produced give a reliable force-displacement curve and deformation mode. Sensitivity studies show that the combination of material properties and simulation parameter offers a relative robust modelling performance (i.e. No significant/abrupt drifting with a small range of perturbation (±10%) in the parameters)

RESULTS

Validation of the FE foot model with foot deformation and plantar pressure distribution data

Standing condition was stimulated and compared to the experimentally measured deformation of the bony structure in order to verify the FE foot model. The displacement of navicular bone represents the foot deformation index in clinical aspect. The node at tuberosity of the navicular bone in medial side was selected, which is normally used as the reference point in manual measurement. The vertical displacement from this node was plotted while the whole bodyweight is applied. Fig. 2 showed the result between the measured navicular drop [31, 32] and FE stimulated result. As shown in the figure, the numerical data showed a reasonable agreement with published data

[31, 32, 33]. Plantar pressure measurement is another common way to analyse different gaits or running styles. Distribution of the pressure on the foot plantar indicates the pattern of gaits and provide a mean to assess the validity and accuracy of the FEM. Fig. 3 shows the distribution of plantar pressure from FEA and platform pressure measurement (Emed pedography platform. Novel GmbH, Munich, Germany) under the static standing load. As shown in the figure, two frames of standing were selected when the GRF is equal to 0.5 body weight (BW), and 1BW, respectively. Pressure distribution from the FE result showed a good agreement with the experimental result measured on the Emed pedography platform. The value of peak pressure between FE and test data match at both the point of 0.5 BW and the full BW load. For the pressure measurement (Fig.3), it should be noted that the system used discrete electrical sensors, then the distribution/contour is formulated through the homogenisation of the reading of all the pressure sensors. From the pressure distribution, it is clear that the global distribution of maxima and minima is similar and maximal stresses are also similar. This suggests that the model is valid in terms of the key aspects of the foot model such as geometry, position of the bones and materials, etc. The pressure values for the heel and forefoot region are also in a general agreement with published data, which will be analysed in details in the discussion section. Navicular bone is the pivoting point of the foot. Its displacement provides a good mean for model validation [34] on works focusing on metatarsals. In the static standing tests, the load was 1BW, for dynamic test, the load was around 2.1BW. During the experiment, for the static standing test, the subject slowly stands on the platform, while for the dynamic test, the subject was asked to hold two parallel bars to lift himself up straight before landing from 100mm height (distance from foot plantar level over the ground) to the rigid ground with full foot contact (i.e. forefoot and rearfoot touching ground at the same time) where the Emed pressure measurement plate was placed. Ground reaction force from Emed plate showed maximum reaction force around average 2.1 body weight. The GRF for standing test is much more reliable, while there is clearly variation in the GRF between different dynamic landing tests as represented by the error bar. However, the average value showed a reasonable agreement between the FE modelling and the tests. The close agreement between the displacement measured in the static standing and dynamic vertical landing tests shows that the model is geometrically sound. The displacement of the proximal end of 1st metatarsal has also been evaluated, the modelling results shows a reasonable agreement with the tests, but the repeatability of the Proximal end of 1st metatarsal is not very reliable, the data was not shown to preserve clarity. These results give more confidence in using the computational model to predict the deformation of the internal bones such as the metatarsals, which cannot be measured directly. Further

discussion on the data is presented in the discussion section to compare the predicted results with other published data under comparable conditions or more challenging situation as well as the limitations of the approach.

Stress distribution on the metatarsals

During the initial touchdown (up to half BW) for forefoot and rearfoot strike, the averaged metatarsal stress is similar around 6MPa. The stress level in the 4th metatarsal in forefoot strike is higher (7.62MPa, Fig. 4), the stress in the 5th metatarsal in rearfoot strike has a much lower value (4.67MPa, Fig. 6). At full contact (2BW), there is a more significant increase in the metatarsal stresses in the forefoot strike, than that for the rearfoot strike. The percentage stress increase from initial touchdown to full contact during rearfoot strike (21.39%) is lower than the rate of increase for forefoot landing (30.76%).

Fig. 4 shows the stress data in the metatarsals between 0.5 BW and 2 BW in forefoot landing. The average metatarsal stress increase is about 30.76% from the initial contact to full contact during forefoot strike. The data shows that the 1st metatarsal experienced the lowest stress at initial touchdown, but the stress increases more significantly with the highest increase rate of 48.21% at full contact. The data for the 5th metatarsal represents the lowest stress increase rate (18%) from the initial touchdown to full contact. Fig. 6 shows the stress data for the rearfoot strike. It can be seen from the data that the 1st metatarsal had the highest stress under both half body weight and twice BW. The highest stress increase rate was presented on the 1st metatarsal during rearfoot strike. The lateral side during rearfoot strike (the 4th and 5th metatarsals) also showed relatively high stress increase rate (10.4% and 11.8%). The stress increases among the five metatarsals shows a more evenly spread along the coronal axis during rearfoot strike than that for forefoot strike.

Deformation of the foot at initial touchdown during forefoot and rearfoot landing is shown in Fig. 5(a) and Fig. 7(a), respectively, the vertical GRF was equal to half BW (350N) at this point. The foot deformation at full contact during forefoot and rearfoot landing is shown in Fig. 5(c) and Fig. 7(c), respectively, the GRF was twice BW (1400N) at this point. Fig. 5(b) and Fig. 5(d) show the stress distribution on the bones at the moment of initial touchdown and full contact, respectively during forefoot landing. Fig. 7(b) and Fig. 7(d) present the bony stress distribution at the moment of initial touchdown and full contact, respectively during rearfoot strike. Compared to full

contact, stress distribution on metatarsals are more evenly distributed at initial touchdown for both landing styles. The 3rd and 4th metatarsals bear higher stress at initial touchdown during forefoot landing (Fig. 5(b)). During rearfoot landing, stress on the metatarsals showed more even distribution at initial touchdown (Fig. 7(b)). For both landing styles, 1st metatarsal showed the highest stress increase rate from the initial touch down to the full contact stage (Fig. 5(d), Fig. 7(d)).

DISCUSSION

As shown in Fig. 2, the numerical results of the FE model are in a good agreement with the experimental data and published works [11,12,13]. The plantar pressure distribution also showed a good agreement between the FE modelling and biomechanical tests. These are commonly used approaches to check the validity and accuracy of FEMs [14, 29, 30]. These will provide confidence in the prediction of the stresses in the metatarsals in forefoot and rearfoot strike, which is the main focus of the work. The GRF on the reference point of rigid plate is used to represent the ground reaction force during whole phase of strike. The trend of the GRF predicted is found to be comparable to other published works [1,3]. The numerical data predicted for both forefoot and rearfoot strike are close to the GRF tests results on the same subject. The peak GRF observed at the end of landing phase for both forefoot and rearfoot strike reaches a similar level (~2.5BW). This is also in agreement with published data, which reported a maximum force of 2.2-2.5 BW [3,5,6]. This load level is also observed by the human body modelling investigating the response of the human body to the collision with the ground during hopping, trotting, or running [35, 36, 37]. In the models, the mass, spring, and damper elements are used to represent the masses, stiffness properties, and damping properties of hard and soft tissues. The reaction force is a combination of the influence of the bodyweight, muscle action, and velocity. The reaction force predicted by the mass-spring-damper model is in a similar range to the load used in the FE models of this work.

The efficiency and stability of an FE explicit model can be verified by checking the ratio between the artificial strain energy and internal energy level (ALLAE/ALLIE), which is commonly used in dynamic situations [38, 39]. It is an indicator for the quality of the mesh size, contact, viscous damping and stabilisation, thus reflecting the accuracy of the solution. In the models developed in this work, the ALLAE/ALLIE ratio is always less than 2% during either forefoot landing or rearfoot strike. This suggests that the FE is effective and stable. As shown in Fig. 8, at 0.5BW load, the

strain energy level stored in the foot is similar between different conditions, and then at 1 BW, the energy for rearfoot strike is slightly higher. While at 2 BW (which is close to the maximum (2.2-2.6 BW) [1], the energy in the foot during rearfoot strike is much higher, this is due to the fact that for rearfoot, the main force is sustained by the bony structure, the heel pad is the main deformable part. For forefoot strike, the soft tissue has a much higher deformation around the metatarsals, which increases the energy stored in the system. These highly strained tissues will cause high stress within the metatarsals as shown in the main results.

This study comparatively evaluated the stress distribution in the metatarsals between forefoot landing and rearfoot strike. As hypothesized, the stress level and increase rate of the metatarsals stresses during forefoot landing is higher than that in rearfoot strike especially. the stress in the 1st metatarsal during forefoot landing is much higher. The results show that a forefoot strike pattern put metatarsals at high stress level along with high rate of stress increase than that for rearfoot strike. The stress distribution and stress level are in agreement with some published data [11, 40]. The case study by Cheung et al. observed a similar result that metatarsal stress increased during barefoot running, which results in severe running injuries, such as metatarsal and calcaneal stress fractures [41]. Giuliani et al [9] reported that metatarsal fracture occurred on novice barefoot runners, which can be explained by the higher loading rate during impact. The landing pattern transition to a forefoot landing style put the metatarsals as the first impact section of the foot [9]. Comparative study of the landing styles revealed the 1st metatarsal has a dominate role bearing relatively high stress and greatest stress increase rate in both forefoot and rearfoot strikes, which is associated with its wider anatomy structure than the other four metatarsals. This is agreeable with the finding of Muehleman et al [42], who mentioned that first Metatarsal bone as a major weight-bearing structure is of important biomechanical function within the foot [42]. During forefoot strike, higher stress increase rate was observed in the medial area of the metatarsals at the 2 BW load point. Whereas, the stresses level at initial contact between each metatarsal during forefoot strike are at a comparable level (around 6MPa). This indicates the automatical pronation has happened under mechanical downwards boundary conditions. In contrast, stress increase is relatively uniform between the five metatarsals during a rearfoot strike.

The model used constraint of ‘embedded region’ to model the key internal foot components encapsulated by hyperelastic material for the soft tissues. The embedded element technique is used to specify that an element or group of elements is embedded

in “host” elements [26]. This offers an effective way of modelling the foot focused on the stresses in the metatarsals with improved efficiency and resource saving. Comparing this with a full perfect contact model without using the embedded region, the number of elements is much lower. For the full modelling approach, the number of element for the whole foot is typically being around 1200000-1300000 [30, 43], which is around 4-5 times the element number used in the current explicit model (273123 elements).

The mechanical response of human foot in different landing conditions have been the subject of many research works [16, 27, 28, 43], in which different procedures have been used to suit the technical focus of the studies. Fontanella et al [27] investigated the mechanical behaviour of the plantar soft tissue during gait cycle using Abaqus implicit modelling. The work considered detailed viscoelastic effects with a specific visco-hyperelastic constitutive model, the mean value of the loading rate during impact is 0.033BW/s, which is close to the loading conditions (0.1s for 2 BW) for this work. In another model by Fontanella et al [43], the tibia and the fibula were considered to be fully fixed, and the boundary and loading condition is simplified by fixing the relative motion between the foot and the plate. Similarly, in the work on the effects of Ankle arthrodesis on biomechanical performance of the entire foot [44, 45], the superior surfaces of the tibia, fibula, and encapsulated soft tissue were fixed throughout the simulation. The ground reaction forces were applied through moving the rigid plate beneath the foot. The pressure at the heel region reported in the works is 0.3-0.33MPa, and 0.22-0.26MPa under the metatarsals. These pressure values are similar to the data predicted in this work. Yu et al [24] conducted biomechanical simulation of high-heeled shoe donning and walking. The work used linear elastic properties for the bone and soft tissues. The average stress in the first metatarsals during the push off phase is around 6.5 MPa at a 1.2 BW, which is similar to the value in this work for forefoot landing. All the works mentioned above used Abaqus implicit, which has limitations in dealing with fast dynamics with small time steps in the landing phase and normally a much higher number of elements are required. Qian [16] used an Abaqus explicit solver with a two-dimensional model to study the human foot complex in the sagittal plane during level walking. Their analysis showed that a dynamic FE simulation can improve the prediction accuracy of the peak plantar pressures at some parts of the foot complex by 10%–33% compared to a quasi-static FE simulation. However, the proposed model is confined only to the sagittal plane and has a simplified representation of foot structure, in which the plane stress section thickness was set to 60 mm representing the approximate foot width of the subject. The FE modelling in this work used a full 3D model, the results show that an explicit model has the advantage of dealing with complex modelling with a more flexible loading to suit different foot loading situations.

The comparison of the stress level between forefoot and rearfoot strike with a subject specific model will provide important information for understanding the loading of metatarsals in different movements. Different peak stress areas indicate the areas more prone to injure on the metatarsals with high stress and increase rate. In particular in forefoot strike, a 9.67% higher stress increase rate in the metatarsals than that for rearfoot strike indicates a higher chance of stress fracture. This agrees with the observation that the forces and stresses experienced in the metatarsal region are increased when using a non-heel strike pattern during running [46]. The bending strain of metatarsals reported by these authors would potentially be increased even higher in those runners selecting to use a non-heel strike running pattern [47]. This may contribute to a higher incidence of metatarsal stress fractures in runners converting to minimalist footwear [9, 10].

Limitation

The work has shown that the use of subject specific modelling can provide a useful tool to compare the foot deformation and stresses in the metatarsals during forefoot and rearfoot strike, in particular for bare foot or with minimalist shoes. There are some limitations of the results, which should be noted and some of which is open to future studies. This paper has been focused on a situation with a rigid ground, this is the same situation as the experiments and represent the most dangerous/relevant situation for metatarsals damage. The results can be extended to more complex situations such as with soils, turfs, etc. This can be either conducted with a layered soft materials system, or more realistically using a discrete element model for modelling the soil. The latter will be able to distinguish the effect of soft ground on the stresses in different metatarsals. The tissue for foot modelling is a complex problem, an optimum scheme has to balance representing the realistic structure, the practicality and efficiency of the modelling. A particular area for the human foot modelling which should be noted is the use of regional properties or age/medical related properties [48]; Our previous work used *in vivo* indentation tests to characterise the soft tissue over different foot zones and used detailed properties in foot modelling [11]; such a process with detailed skin behaviours [27] and heel pad properties [43, 49, 50, 51] should be adapted when the plantar pressure is the main focus of the modelling for situation such as diabetes feet. Another area should be noted is the modelling of the bone. This study has focused on the whole deformation of the foot bony structure in standing, forefoot and rearfoot landing. The bone has been modelled with a uniform property. This is probably sufficient for studying the general stress levels in the metatarsals, further details are required to extend the modelling to more complex loading conditions or more

challenging landing situations such as inversion and eversion landing. For detailed modelling of the metatarsals, more detailed works are required, ideally using submodelling to extract the boundary condition and force around the metatarsals, in which the individual muscle, even nerve can be considered. This is will be addressed in future works.

CONCLUSION

This work presents a detailed study in developing an effective finite element (FE) modelling approach to comparatively study the stresses and energy in the foot during forefoot strike (FS) and rearfoot strike (RS). An explicit solver was used to stimulate the transient landing process of the foot to improve the convergence and modelling efficiency. The results for the forefoot strike tests showed an overall higher average stress level in the metatarsals during forefoot landing than that for rearfoot strike. The metatarsal stress increased 30.76% for forefoot strike and 21.39% for rearfoot strike when the load is increased from 0.5 body weight (BW) to 2 BW. The maximum rate of stress increase in the five metatarsals is observed on the first metatarsal in both landing modes. During forefoot landing, the average stress on the first metatarsal is increased by 48.21% from 0.5BW to 2BW. The results indicate that changing strike pattern from rearfoot strike to forefoot may increase the potential of metatarsals injuries due to the high stress level and stress increase rate.

Acknowledgements
This study sponsored by National Natural Science Foundation of China (81772423), and K. C. Wong Magna Fund in Ningbo University.

References

[1] D. E. Lieberman, "What we can learn about running from barefoot running: an evolutionary medical perspective," *Exercise and sport sciences reviews,* vol. 40, pp. 63-72, 2012
[http://dx.doi.org/10.1097/JES.0b013e31824ab210] [PMID: 22257937]

[2] Y. Shih, K.-L. Lin, and T.-Y. Shiang, "Is the foot striking pattern more important than barefoot or shod conditions in running?" *Gait & posture,* vol. 38, pp. 490-494, 2013
[http://dx.doi.org/10.1016/j.gaitpost.2013.01.030] [PMID: 23507028]

[3] D. E. Lieberman, M. Venkadesan, W. A. Werbel, A. I. Daoud, S. D'Andrea, I. S. Davis, *et al.*, "Foot strike patterns and collision forces in habitually barefoot versus shod runners," *Nature,* vol. 463, pp. 531-535, 2010
[http://dx.doi.org/10.1038/nature08723]

[4] C. Divert, G. Mornieux, H. Baur, F. Mayer, and A. Belli, "Mechanical comparison of barefoot and shod running," *International journal of sports medicine,* vol. 26, pp. 593-598, 2005
[http://dx.doi.org/10.1055/s-2004-821327]

[5] R. Squadrone, C. Gallozzi, "Biomechanical and physiological comparison of barefoot and two shod conditions in experienced barefoot runners," *Journal of Sports Medicine and Physical Fitness,* vol. 49, pp. 6, 2009
[PMID: 19188889]

[6] H. P. Crowell and I. S. Davis, "Gait retraining to reduce lower extremity loading in runners," *Clinical biomechanics,* vol. 26, pp. 78-83, 2011
[http://dx.doi.org/10.1016/j.clinbiomech.2010.09.003]

[7] A. I. Daoud, G. J. Geissler, F. Wang, J. Saretsky, Y. A. Daoud, and D. E. Lieberman, "Foot strike and injury rates in endurance runners: a retrospective study," *Medicine & Science in Sports & Exercise,* vol. 44, pp. 1325-34, 2012

[http://dx.doi.org/ 10.1249/MSS.0b013e3182465115]

[8] T. Kernozek, S. Meardon, and C. Vannatta, "In-shoe loading in rearfoot and non-rearfoot strikers during running using minimalist footwear," *International journal of sports medicine,* vol. 35, pp. 1112-1117, 2014
[http://dx.doi.org/10.1055/s-0034-1372627]

[9] J. Giuliani, B. Masini, C. Alitz, and L. B. D. Owens, "Barefoot-simulating footwear associated with metatarsal stress injury in 2 runners," *Orthopedics,* vol. 34, pp. e320-e323, 2011
[http://dx.doi.org/10.3928/01477447-20110526-25]

[10] M. J. Salzler, E. M. Bluman, S. Noonan, C. P. Chiodo, and R. J. de Asla, "Injuries observed in minimalist runners," *Foot & Ankle International,* vol. 33, pp. 262-266, 2012
[http://dx.doi.org/10.3113/FAI.2012.0262]

[11] Y. Gu, X. Ren, G. Ruan, Y. Zeng, and J. Li, "Foot contact surface effect to the metatarsals loading character during inversion landing," *International Journal for Numerical Methods in Biomedical Engineering,* vol. 27, pp. 476-484, 2011
[http://dx.doi.org/10.1002/cnm.1414]

[12] J. T.-M. Cheung, M. Zhang, A. K.-L. Leung, and Y.-B. Fan, "Three-dimensional finite element analysis of the foot during standing—a material sensitivity study," *Journal of biomechanics,* vol. 38, pp. 1045-1054, 2005
[http://dx.doi.org/10.1016/j.jbiomech.2004.05.035] [PMID: 15797586]

[13] J. T.-M. Cheung and M. Zhang, "Finite element modelling of the human foot and footwear," in *ABAQUS users' conference*, pp. 145-159. 2006

[14] A. Guiotto, Z. Sawacha, G. Guarneri, A. Avogaro, and C. Cobelli, "3D finite element model of the diabetic neuropathic foot: a gait analysis driven approach," *Journal of biomechanics,* vol. 47, pp. 3064-3071, 2014
[http://dx.doi.org/10.1016/j.jbiomech.2014.06.029] [PMID: 25113808]

[15] W. B. Edwards, D. Taylor, T. J. Rudolphi, J. C. Gillette, and T. R. Derrick, "Effects of running speed on a probabilistic stress fracture model," *Clinical Biomechanics*, vol. 25, pp. 372-377, 2010 [http://dx.doi.org/10.1016/j.clinbiomech.2010.01.001]

[16] Z. Qian, L. Ren, Y. Ding, J. R. Hutchinson, L. Ren, "A dynamic finite element analysis of human foot complex in the sagittal plane during level walking, " *PloS one*, Vol8(11), e79424, 2013.

[17] H. Zhao, S. Li, L. Li, G. Rothwell, & J. Ren, "Numerical modelling and analytical analysis of Shore OO hardness tests on soft materials," *International Journal of Experimental and Computational Biomechanics*, vol.*4*(1), pp.1-12, 2016.

[18] S.D. Li, K. Al-Badani1, Y.D. Gu, M. Lake, L. Li, G. Rothwel and J. Ren, "The Effects of Poisson's Ratio on the Indentation Behaviour of Materials with Embedded System in an Elastic Matrix," in press

[19] M. Kazemi, Y. Dabiri, and L. P. Li, 2015, "Recent Advances in Computational Mechanics of the Human Knee Joint." *Computational and Mathematical Methods in Medicine*, 2013, p1-27.

[20] A. Wittek, K. Miller, R. Kikinis, and S.K. Warfield, "Patient-specific model of brain deformation: Application to medical image registration." *Journal of biomechanics*, vol. 40 no.4, pp.919-929, 2007.

[21] F. Auricchio, M. Conti, S. Marconi, A. Reali, J.L. Tolenaar, and S. Trimarchi, "Patient-specific aortic endografting simulation: From diagnosis to prediction." *Computers in biology and medicine*, vol. 43 no.4, pp.386-394, 2013.

[22] K. Hibbitt, & Sorensen, *ABAQUS/Explicit User's Manual*. Version 6.14. Pawtucket: Hibbitt, Karlsson & Sorensen, Inc. 2014

[23] S. Nakamura, R. Crowninshield, and R. Cooper, "An analysis of soft tissue loading in the foot--a preliminary report," *Bulletin of prosthetics research*, vol.10, pp. 27-34, 1980.

[24] J. Yu, J.T. Cheung JT, D.W. Wong, Y. Cong, M. Zhang, "Biomechanical simulation of high-heeled shoe donning and walking," *Journal of Biomechanics*, vol.46 pp.2067-2074, 2013

[25] D. Lemmon, T.-Y. Shiang, A. Hashmi, J. S. Ulbrecht, and P. R. Cavanagh, "The effect of insoles in therapeutic footwear—a finite element approach," *Journal of biomechanics*, vol. 30, pp. 615-620, 1997 [PMID: 9165395]

[26] Abaqus User's Manual, Version 6.14, Dassault Systèmes Simulia Corp., Providence, RI. section 15.15.8 and section 35.4.1 (embedded elements). 2014

[27] C.G. Fontanella, A. Forestiero, E.L. Carniel, A.N. Natali, "Investigation of the mechanical behaviour of the plantar soft tissue during gait cycle: experimental and numerical investigation, " Proceedings of the Institution of Mechanical

Engineers, Part H: *Journal of Engineering in Medicine*, vol.229(10), pp. 713-720, 2015

[28] T. X. Qiu, , E. C Teo, Y. B. Yan, W. Lei, "Finite element modelling of a 3D coupled foot–boot model," *Medical engineering & physics*, vol.33(10), pp.1228-1233. 2011

[29] A. Erdemir, J. J. Saucerman, D. Lemmon, B. Loppnow, B. Turso, J. S. Ulbrecht, "Local plantar pressure relief in therapeutic footwear: design guidelines from finite element models," *Journal of biomechanics*, vol. 38, pp. 1798-1806, 2005. [http://dx.doi.org/10.1016/j.jbiomech.2004.09.009]

[30] Y. D. Gu, X. J. Ren, J. S. Li, M. J. Lake, Q. Y. Zhang, Y. J. Zeng, 2010, "Computer simulation of stress distribution in the metatarsals at different inversion landing angles using the finite element method," *International Orthopaedics* June Vol 34, Issue 5, pp.669–676, 2010

[31] R. G. Nielsen, M. S. Rathleff, O. H. Simonsen, and H. Langberg, "Determination of normal values for navicular drop during walking: a new model correcting for foot length and gender," *Journal of foot and ankle research*, vol. 2, pp.12, 2009
[http://dx.doi.org/10.1186/1757-1146-2-12]

[32] A. M. Picciano, M. S. Rowlands, and T. Worrell, "Reliability of open and closed kinetic chain subtalar joint neutral positions and navicular drop test," *Journal of Orthopaedic & Sports Physical Therapy*, vol. 18, pp.553-558, 1993. [http://dx.doi.org/10.2519/jospt.1993.18.4.553]

[33] J. L. Moul, "Differences in selected predictors of anterior cruciate ligament tears between male and female NCAA Division I collegiate basketball players," *Journal of athletic training*, vol. 33, pp. 118, 1998
[PMC1320397]

[34] M. J. Mueller, J. V. Host, B. J. Norton, "Navicular drop as a composite measure of excessive pronation," *Journal of the American Podiatric Medical Association*, vol.83(4), pp.198-202, 1993

[35] A. Nikooyan, A. Zadpoor, 2012, "Effects of Muscle Fatigue on the Ground Reaction Force and Soft-Tissue Vibrations During Running: A Model Study , "Published in: IEEE Transactions on Biomedical Engineering Vol59 (3), March 2012

[36] K. P. Clark, L. J. Ryan, P. G. Weyand, "A general relationship links gait mechanics and running ground reaction forces," *Journal of Experimental Biology* vol. 220 pp. 247-258, 2017
[doi: 10.1242/jeb.138057]

[37] N. Nedergaard, M. Robinson, B. Drust, P. Lisboa, J. Vanrenterghem, "Predicting ground reaction forces from trunk kinematics: A mass-spring-damper model approach, " *International Society of Biomechanics Conference Proceedings*, vol.1 (1) pp.432-435, 2017

[38] F. Auricchio, M. Conti, M. De Beule, G. De Santis, and B. Verhegghe, "Carotid artery stenting simulation: from patient-specific images to finite element analysis," *Medical engineering & physics*, vol.33, pp.281-289, 2011 [http://dx.doi.org/10.1016/j.medengphy.2010.10.011] [PMID: 21067964]

[39] B. Egan, M. McCarthy, R. Frizzell, P. Gray, and C. McCarthy, "Modelling bearing failure in countersunk composite joints under quasi-static loading using 3D explicit finite element analysis," *Composite Structures*, vol. 108, pp. 963-977, 2014 [http://dx.doi.org/10.1016/j.compstruct.2013.10.033]

[40] D. W.-C. Wong, Y. Wang, M. Zhang, and A. K.-L. Leung, "Functional restoration and risk of non-union of the first metatarsocuneiform arthrodesis for hallux valgus: a finite element approach," *Journal of biomechanics*, vol. 48, pp. 3142-3148, 2015 [http://dx.doi.org/10.1016/j.jbiomech.2015.07.013] [PMID: 26243661]

[41] R. T. Cheung and M. J. Rainbow, "Landing pattern and vertical loading rates during first attempt of barefoot running in habitual shod runners," *Human movement science*, vol. 34, pp. 120-127, 2014 [http://dx.doi.org/10.1016/j.humov.2014.01.006] [PMID: 24556474]

[42] C. Muehleman, R. Lidtke, A. Berzins, J. Becker, S. Shott, and D. Sumner, "Contributions of bone density and geometry to the strength of the human second metatarsal," *Bone*, vol. 27, pp. 709-714, 2000. [http://dx.doi.org/10.1016/S8756-3282(00)00370-7]

[43] C.G. Fontanella, E.L. Carniel, A. Forestiero, A.N. Natali, "Investigation of the mechanical behaviour of foot skin," *Skin Research & Technology*, vol.20, pp.445-452. 2014

[44] J. T. M. Cheung, M. Zhang, "Parametric design of pressure-relieving foot orthosis using statistics-based finite element method, " *Medical Engineering & Physics* vol. 30 pp.269–277, 2008

[45] Y. Wang, L. Zengyong, D.W. Wong, M. Zhang, "Effects of ankle arthrodesis on biomechanical performance of the entire foot, " *Plos one*, vol.10(7), pp.1-22, 2015 [DOI: 10.1371/journal.pone.0134340]

[46] T. W. Kernozek, C. N. Vannatta, N. Gheidi, S. Kraus, and N. Aminaka, "Plantar loading changes with alterations in foot strike patterns during a single session in habitual rear foot strike female runners," *Physical Therapy in Sport*, vol.18, pp. 32-37, 2016 [http://dx.doi.org/10.1016/j.ptsp.2015.05.004] [PMID:26803672]

[47] T. S. Gross and R. Bunch, "A mechanical model of metatarsal stress fracture during distance running," *The American journal of sports medicine*, vol. 17, pp. 669-674, 1989

[48] W.R. Ledoux, J.J. Blevins, "The compressive material properties of the plantar soft tissue". *Journal of Biomechanics*, vol. 40 pp.2975-2981, 2007

[49] A. N. Natali, C. G. Fontanella, E. L. Carniel, J. M. Young, "Biomechanical behaviour of heel pad tissue: Experimental testing, constitutive formulation, and numerical modelling". Proceedings of the Institution of Mechanical Engineers, Part H: *Journal of Engineering in Medicine*, vol.225, pp.449-459, 2011

[50] A. N. Natali, C. G. Fontanella, E. L. Carniel, "Constitutive formulation and numerical analysis of the heel pad region," *Computer Methods in Biomechanics and Biomedical Engineering*, vol. 15 pp.401-409, 2012

[51] C.G. Fontanella, S. Matteoli, E.L. Carniel, J.E., Wilhjel, A. Virga, A. Corvi, A.N. Natali, "Investigation on the load-displacement curves of a human healthy heel pad: in vivo compression data compared to numerical results," *Medical Engineering and Physics*. 34: 1253-1259. 2012.

Fig. 1 Process of building FE model with hexahedral elements from 2D CT image to Abaqus Explicit.

Fig. 2 Comparison of vertical navicular displacement between FE prediction, experimental data and published data.

Fig. 3 Comparison between FE prediction and experimental data of Plantar pressure under standing load.

Fig. 4 Stress on metatarsals at half and twice Body weight (BW) during forefoot strike.

Fig. 5 Typical FE data for Forefoot strike. (a) Deformation in sagittal plane at initial touchdown (0.5BW), (b) stress distribution in axial plane at initial touching-down, (c) deformation in sagittal plane at full contact (2BW), (d) stress distribution in axial plane at full contact.

Fig. 6 Stress on metatarsals at half and twice BW during rearfoot strike.

Fig. 7 Typical FE data for Rearfoot strike. (a) Deformation in sagittal plane at initial touchdown (0.5BW), (b) stress distribution in axial plane at initial touching-down, (c) deformation in sagittal plane at full contact (2BW), (d) stress distribution in axial plane at full contact.

Fig. 8 Comparison of the strain energy level of the foot during standing, forefoot and rearfoot strike. The strain energy of the foot represents the nature energy absorption.

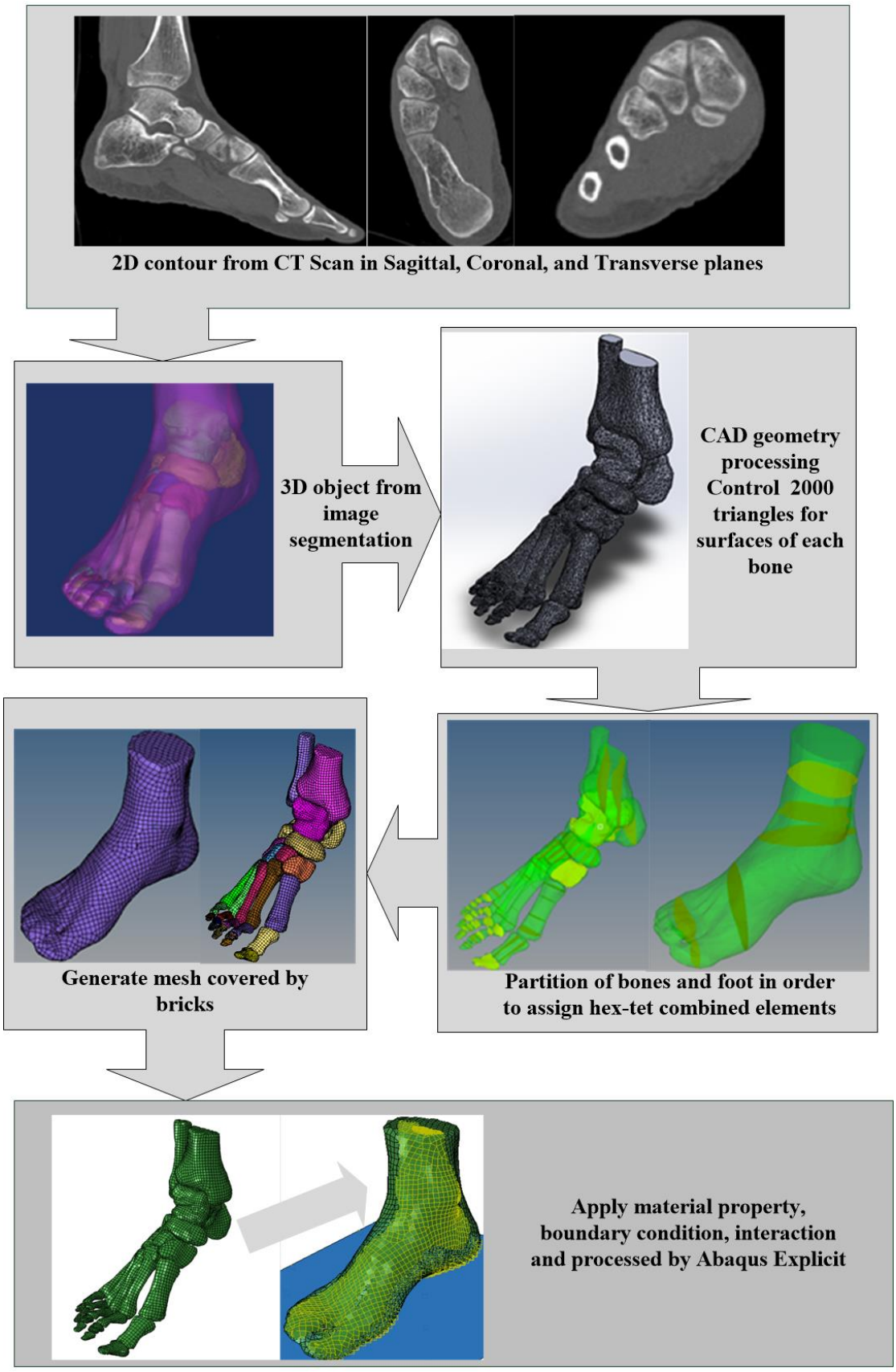
2D contour from CT Scan in Sagittal, Coronal, and Transverse planes
3D object from image segmentation
CAD geometry processing Control 2000 triangles for surfaces of each bone
Partition of bones and foot in order to assign hex-tet combined elements
Generate mesh covered by bricks
Apply material property, boundary condition, interaction and processed by Abaqus Explicit

Figure 1

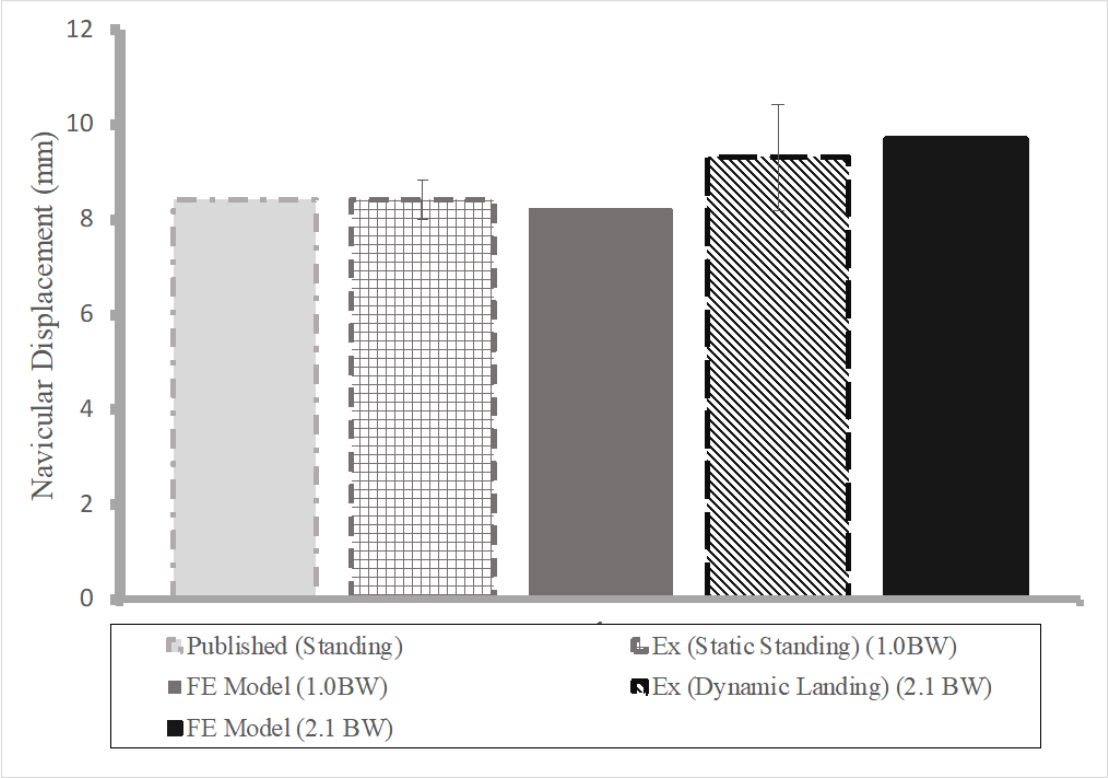
Navicular Displacement (mm)
12
10
8
6
4
2
0
Published (Standing)
Ex (Static Standing) (1.0BW)
FE Model (1.0BW)
Ex (Dynamic Landing) (2.1 BW)
FE Model (2.1 BW)

Figure 2

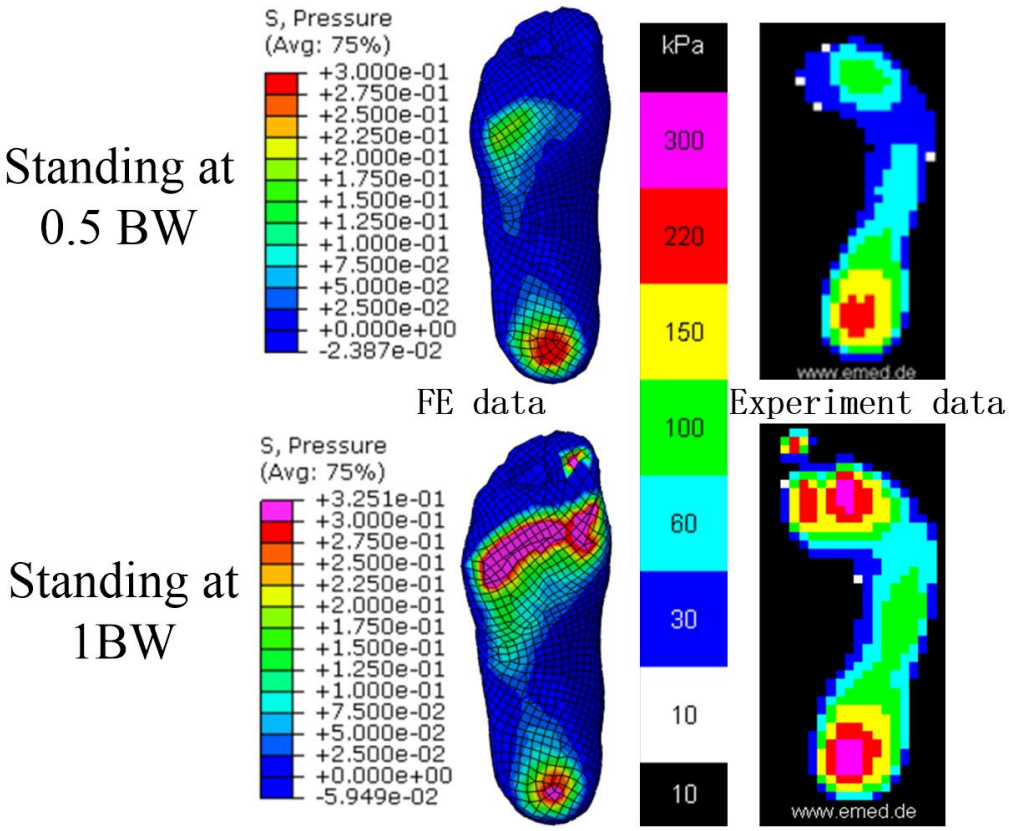
Standing at 0.5 BW
S, Pressure
(Avg: 75%)
+3.000e-01
+2.750e-01
+2.500e-01
+2.250e-01
+2.000e-01
+1.750e-01
+1.500e-01
+1.250e-01
+1.000e-01
+7.500e-02
+5.000e-02
+2.500e-02
+0.000e+00
-2.387e-02
FE data
kPa
300
220
150
100
60
30
10
10
www.emed.de
Experiment data
Standing at 1BW
S, Pressure
(Avg: 75%)
+3.251e-01
+3.000e-01
+2.750e-01
+2.500e-01
+2.250e-01
+2.000e-01
+1.750e-01
+1.500e-01
+1.250e-01
+1.000e-01
+7.500e-02
+5.000e-02
+2.500e-02
+0.000e+00
-5.949e-02
www.emed.de

Figure 3

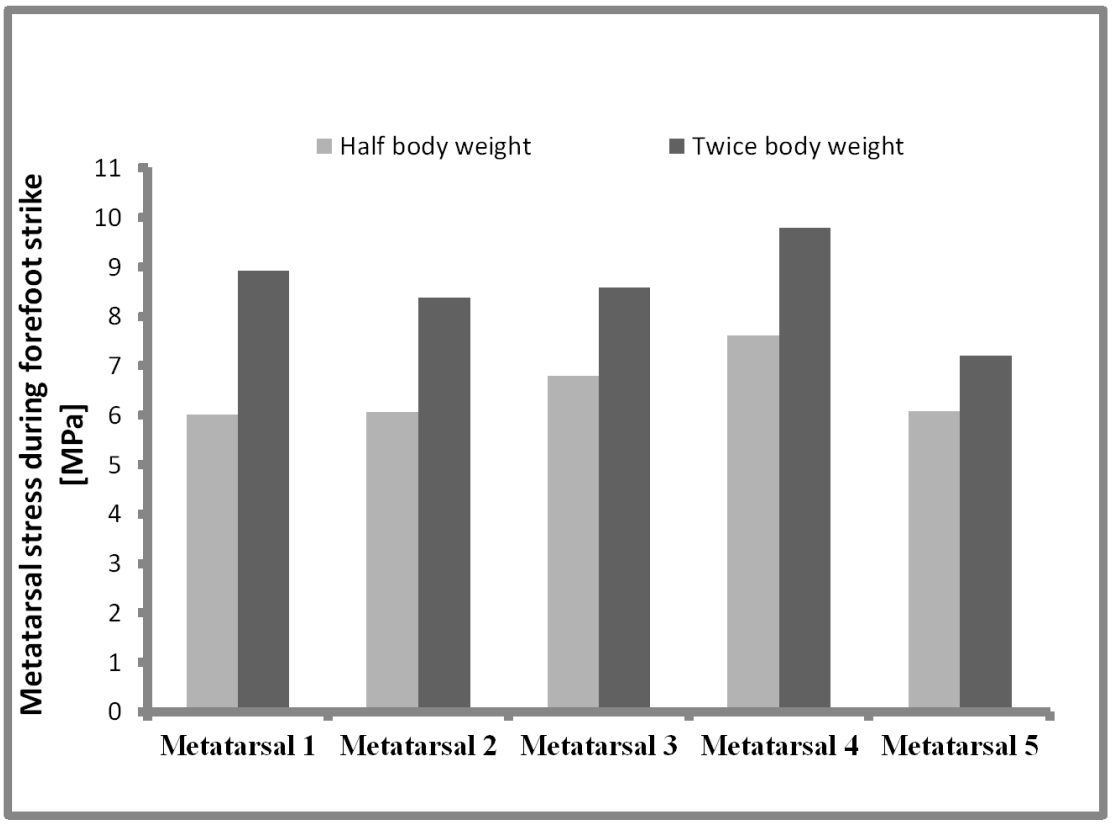
Half body weight
Twice body weight
Metatarsal stress during forefoot strike [MPa]
11
10
9
8
7
6
5
4
3
2
1
0
Metatarsal 1
Metatarsal 2
Metatarsal 3
Metatarsal 4
Metatarsal 5

Figure 4

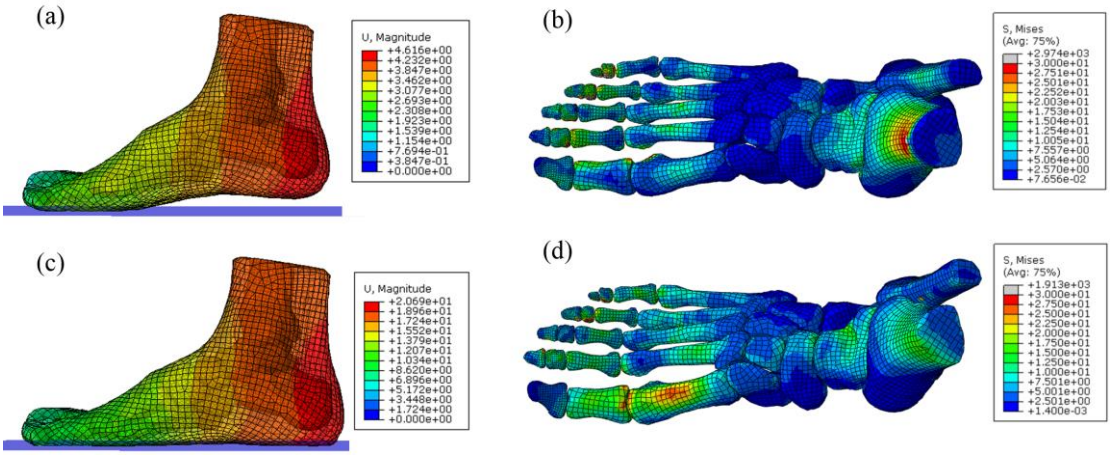
(a)
U, Magnitude
+4.616e+00
+4.232e+00
+3.847e+00
+3.462e+00
+3.077e+00
+2.693e+00
+2.308e+00
+1.923e+00
+1.539e+00
+1.154e+00
+7.694e-01
+3.847e-01
+0.000e+00
(b)
S, Mises
(Avg: 75%)
+2.974e+03
+3.000e+01
+2.751e+01
+2.501e+01
+2.252e+01
+2.003e+01
+1.753e+01
+1.504e+01
+1.254e+01
+1.005e+01
+7.557e+00
+5.064e+00
+2.570e+00
+7.656e-02
(c)
U, Magnitude
+2.069e+01
+1.896e+01
+1.724e+01
+1.552e+01
+1.379e+01
+1.207e+01
+1.034e+01
+8.620e+00
+6.896e+00
+5.172e+00
+3.448e+00
+1.724e+00
+0.000e+00
(d)
S, Mises
(Avg: 75%)
+1.913e+03
+3.000e+01
+2.750e+01
+2.500e+01
+2.250e+01
+2.000e+01
+1.750e+01
+1.500e+01
+1.250e+01
+1.000e+01
+7.501e+00
+5.001e+00
+2.501e+00
+1.400e-03

Figure 5

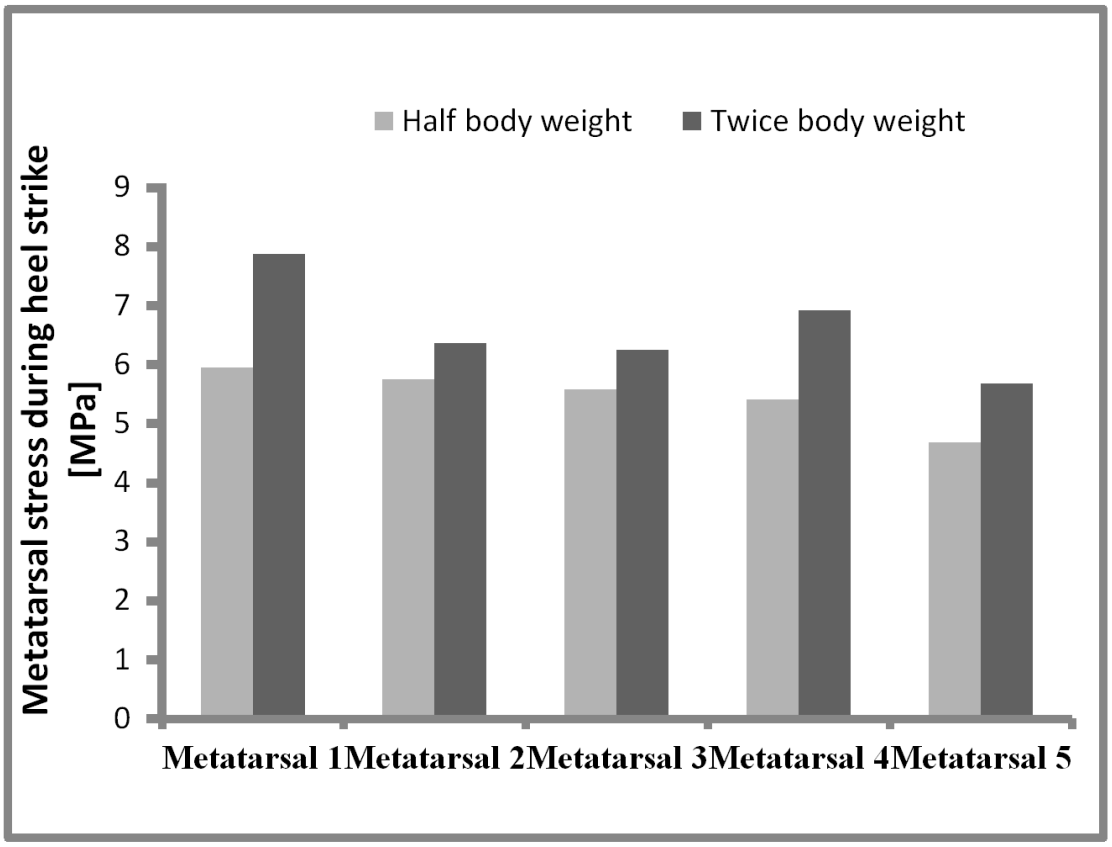
Half body weight
Twice body weight
Metatarsal stress during heel strike [MPa]
9
8
7
6
5
4
3
2
1
0
Metatarsal 1
Metatarsal 2
Metatarsal 3
Metatarsal 4
Metatarsal 5

Figure 6

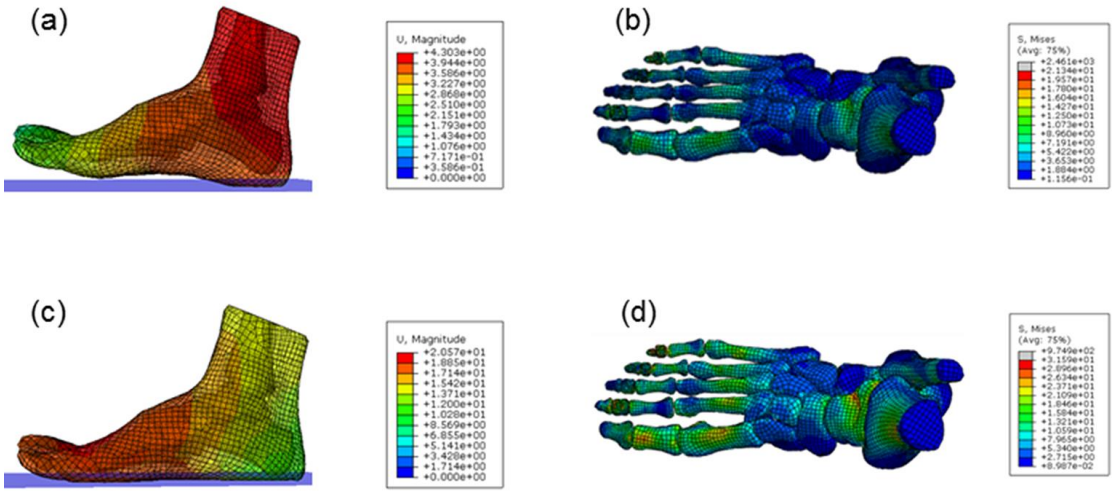
(a)
U, Magnitude
+4.303e+00
+3.944e+00
+3.586e+00
+3.227e+00
+2.868e+00
+2.510e+00
+2.151e+00
+1.793e+00
+1.434e+00
+1.076e+00
+7.171e-01
+3.586e-01
+0.000e+00
(b)
S, Mises
(Avg: 75%)
+2.461e+03
+2.134e+01
+1.957e+01
+1.780e+01
+1.604e+01
+1.427e+01
+1.250e+01
+1.073e+01
+8.960e+00
+7.191e+00
+5.422e+00
+3.653e+00
+1.884e+00
+1.156e-01
(c)
U, Magnitude
+2.057e+01
+1.885e+01
+1.714e+01
+1.542e+01
+1.371e+01
+1.200e+01
+1.028e+01
+8.569e+00
+6.855e+00
+5.141e+00
+3.428e+00
+1.714e+00
+0.000e+00
(d)
S, Mises
(Avg: 75%)
+9.749e+02
+3.159e+01
+2.896e+01
+2.634e+01
+2.371e+01
+2.109e+01
+1.846e+01
+1.584e+01
+1.321e+01
+1.059e+01
+7.965e+00
+5.340e+00
+2.715e+00
+8.987e-02

Figure 7

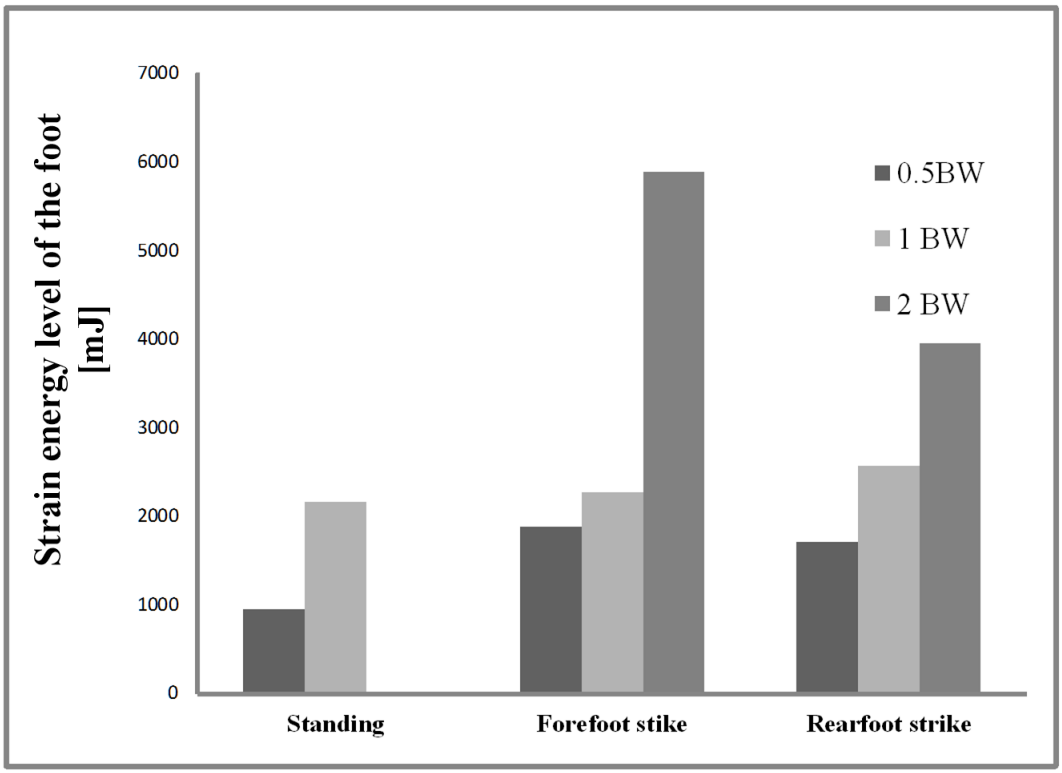
Strain energy level of the foot [mJ]
7000
6000
5000
4000
3000
2000
1000
0
0.5BW
1 BW
2 BW
Standing
Forefoot stike
Rearfoot strike